ORIGINAL PAPER

Failure Behaviour of a Sandstone Subjected to the Systematic Cyclic Loading: Insights from the Double-Criteria Damage-Controlled Test Method

Roohollah Shirani Faradonbeh[1] · Abbas Taheri[1] · Murat Karakus[1]

Abstract
The post-peak behaviour of rocks subjected to cyclic loading is very significant to appraise the long-term stability of underground excavations. However, an appropriate testing methodology is required to control the damage induced by the cyclic loading during the failure process. In this study, the post-failure behaviour of Gosford sandstone subjected to the systematic cyclic loading at different stress levels was investigated using the double-criteria damage-controlled testing methodology, and the complete stress–strain relations were captured successfully. The results showed that there exists a fatigue threshold stress in the range of 86–87.5% of the average monotonic strength in which when the cyclic loading stress is below this threshold, no failure occurred for a large number of cycles and in turn, the peak strength improved up to 8%. Also, the variation of the energy dissipation ratio, rock stiffness and acoustic emission hits for hardening tests showed that cyclic loading in the pre-peak regime creates no critical damage in the specimen, and a quasi-elastic behaviour dominates the damage evolution. The post-failure instability of such tests was similar to those obtained for monotonic tests. On the other hand, by exceeding the fatigue threshold stress, the brittleness of the specimens increased with an increase in the applied stress level, and class II behaviour prevailed over total post-peak behaviour. A loose-dense-loose behaviour with different extents was also observed in the post-peak regime of all fatigue cyclic loading tests. This was manifested then as a secondary inverted S-shaped damage behaviour by the variation of the cumulative irreversible axial and cumulative irreversible lateral strains with the post-peak cycle number. Furthermore, it was confirmed that the damage per cycle in the post-peak regime decreases exponentially with an increase in the applied stress level.

Keywords Pre-peak and post-peak behaviour · Systematic cyclic loading · Brittleness · Hardening · Fatigue · Damage evolution

List of symbols

$E_{\tan}$	Tangent Young's modulus
v	Poisson's ratio
σ_1	Major principal stress
σ_a	Axial stress
σ_i	Indicator stress
$\sigma_{a-\mathrm{peak}}$	Axial peak stress
σ_m	Average monotonic strength
σ_a/σ_m	Applied stress level
σ_h/σ_m	Strength hardening ratio
$\sigma_{ci}/\sigma_{a-\mathrm{peak}}$	Crack initiation stress ratio
$\sigma_{cd}/\sigma_{a-\mathrm{peak}}$	Crack damage stress ratio
ε_a	Axial strain
ε_l	Lateral strain
$d\varepsilon_l/dt$	Lateral strain rate
$\varepsilon_{a-\mathrm{peak}}$	Axial strain at peak stress
$\varepsilon_{l-\mathrm{peak}}$	Lateral strain at peak stress
$\varepsilon_{v-\mathrm{peak}}$	Volumetric strain at peak stress
ε_{a-f}	Axial strain at the final cycle
$\varepsilon_a^{\mathrm{irr}}$	Irreversible axial strain
$\varepsilon_l^{\mathrm{irr}}$	Irreversible lateral strain
$\Sigma\varepsilon_a^{\mathrm{irr}}$	Cumulative irreversible axial strain
$\Sigma\varepsilon_l^{\mathrm{irr}}$	Cumulative irreversible lateral strain
U_e	Elastic energy at peak stress

✉ Roohollah Shirani Faradonbeh
  roohollah.shiranifaradonbeh@adelaide.edu.au

  Abbas Taheri
  abbas.taheri@adelaide.edu.au

  Murat Karakus
  murat.karakus@adelaide.edu.au

1 School of Civil, Environmental and Mining Engineering, The University of Adelaide, Adelaide, SA 5005, Australia
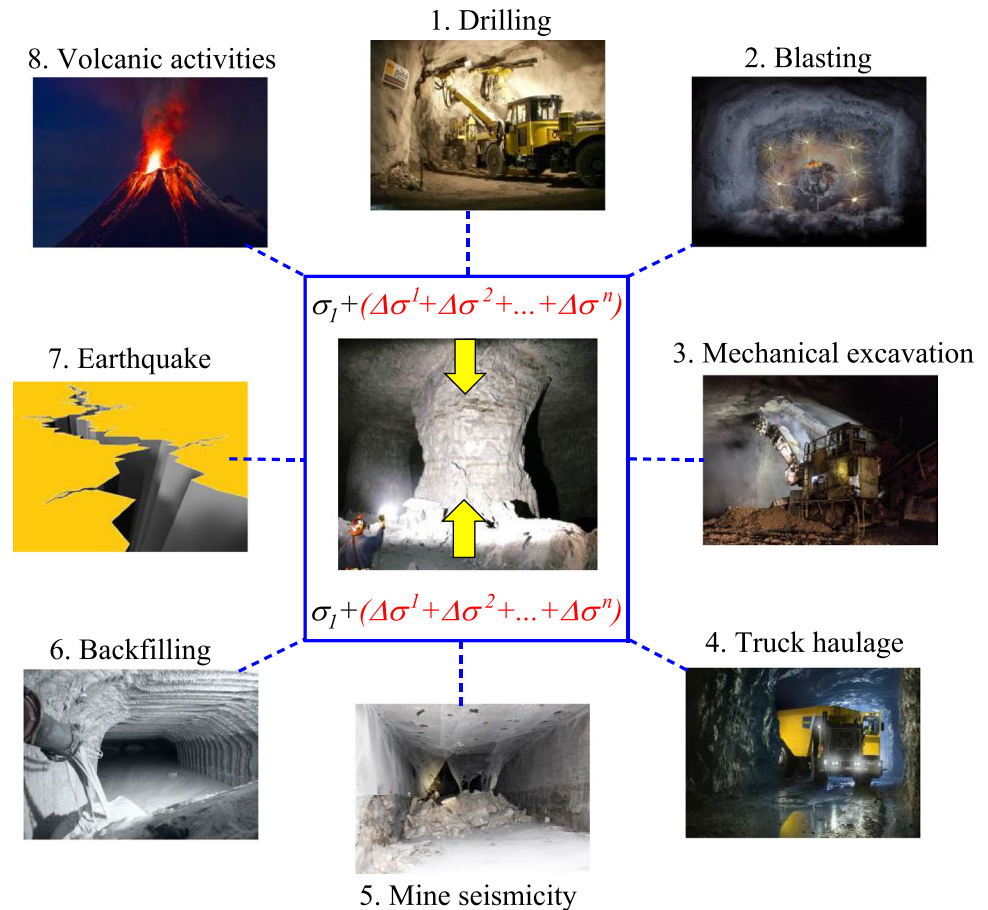
U_e^i	Elastic energy of cycle i
U_d^i	Dissipated energy of cycle i
U_{pre}	Pre-peak dissipated energy
U_{post}	Post-peak dissipated energy
U_t	Total fracture energy
Amp. (σ_a)	Loading amplitude
Amp. (ε_l)	Lateral strain amplitude
n	Cycle number
N_{total}	Total number of cycles
N_{after}	Number of cycles after failure point
BI	Brittleness index
D	Damage variable
M	Post-peak modulus

1 Introduction

A high-complex stress state usually is created around deep-buried tunnels and caverns due to disturbances induced by different sources as displayed in Fig. 1. This stress state may affect mechanical rock properties and in turn, cause some specific failure phenomena such as slabbing/spalling, strainburst and zonal disintegration significantly different from those in shallow conditions (Gong et al. 2012; Shirani Faradonbeh and Taheri 2019). According to Martin and Chandler (1994) and Martin (1997), the surrounding rocks in underground excavations may experience load-and-deformation response to a different extent during operation, and rock may be exposed to cyclic loading. In particular, they argued that in remote to nearby excavation regions, rock may experience failure (i.e. the applied stress level exceeds the peak strength), damage (i.e. the applied stress is below the peak strength) or disturbance (i.e. different stress is applied due to the redistribution of the in-situ stresses) or the rock may remain undisturbed. From this viewpoint, the rock cyclic load-deformation response may take place in the pre-peak or post-peak regime (Munoz and Taheri 2019). For instance, as depicted in Fig. 1, a pillar may experience cyclic loading due to blasting operation or other seismic activities beyond the limit in uniaxial conditions. Under such loading conditions, rock materials may still keep some loadings even in the post-failure regime. Therefore, the investigation of the pre-peak and post-peak behaviour of rocks is of paramount significance to understand more about the fracturing mechanism, resilient design and long-term stability assessment of the various rock engineering structures subjected to seismic disturbances. Experimental research on the influence


Fig. 1 Different sources of seismic disturbances imposing on an underground mining pillar, σ_1 corresponds to the major in-situ stress and $\Delta\sigma^i$ refers to the cyclic loadings originated from different sources

8. Volcanic activities

1. Drilling

2. Blasting

$\sigma_1+(\Delta\sigma^1+\Delta\sigma^2+...+\Delta\sigma^n)$

7. Earthquake

3. Mechanical excavation

$\sigma_1+(\Delta\sigma^1+\Delta\sigma^2+...+\Delta\sigma^n)$

6. Backfilling

4. Truck haulage

5. Mine seismicity

of cyclic loading parameters on the damage evolution and rock strength and deformation parameters has a long tradition. These studies have been conducted under different loading histories and loading conditions such as uniaxial and triaxial compression tests (Heap and Faulkner 2008; Heap et al. 2009; Liu et al. 2018), indirect tensile tests (Erarslan et al. 2014; Wang et al. 2016), flexural tests (Cattaneo and Labuz 2001; Cardani and Meda 2004) and freeze–thaw tests (Liu et al. 2015; Zhang et al. 2019). A comprehensive review of the rock fatigue studies can be found in Cerfontaine and Collin (2018). The majority of prior rock fatigue studies have emphasised the strength weakening of rocks due to incurring permanent deformations during cyclic loading (Haimson 1978; Fuenkajorn and Phueakphum 2010). However, very few studies have reported the strength improvement when the stress level that cyclic loading is applied is low enough to prevent failure (Singh 1989; Ma et al. 2013; Taheri et al. 2017). In prior studies, the process of damage evolution and the failure mechanism of rocks subjected to different cyclic loading histories have been investigated based on the measured stress–strain relations (Cerfontaine and Collin 2018). Indeed, the complete stress–strain relation of rocks (i.e. the pre-peak and the post-peak regimes) is considered as a prominent tool in rock engineering to

describe strain energy evolution as well as for rock brittleness determination (Munoz et al. 2016a; Shirani Faradonbeh et al. 2020). According to Wawersik and Fairhurst (1970), the post-peak behaviour of rocks under quasi-static compression can be distinguished into two classes: (a) class I which is characterised by the negative post-peak modulus (i.e. $M = d\sigma/d\varepsilon < 0$) representing the gradual strength degradation of rock specimen and the need for extra energy and (b) class II having a positive post-peak modulus represents the self-sustaining failure with strain recovery and release of excess elastic strain energy. The proper measurement of the complete stress–strain response of rocks significantly depends on the stiffness of the loading system, the applied load controlling technique throughout the test as well as rock brittleness (Wawersik and Fairhurst 1970; Munoz and Taheri 2019).

Shirani Faradonbeh et al. (2020) categorised the cyclic loading methods based on the loading histories and load control variables into two main groups of systematic cyclic loading (single-level or multi-level) (Fig. 2a, b) and damage-controlled cyclic loading (load-based or displacement-based) (Fig. 2c, d). Systematic cyclic loading can be conducted under load-controlled or displacement-controlled loading conditions. In both loading conditions, a sudden
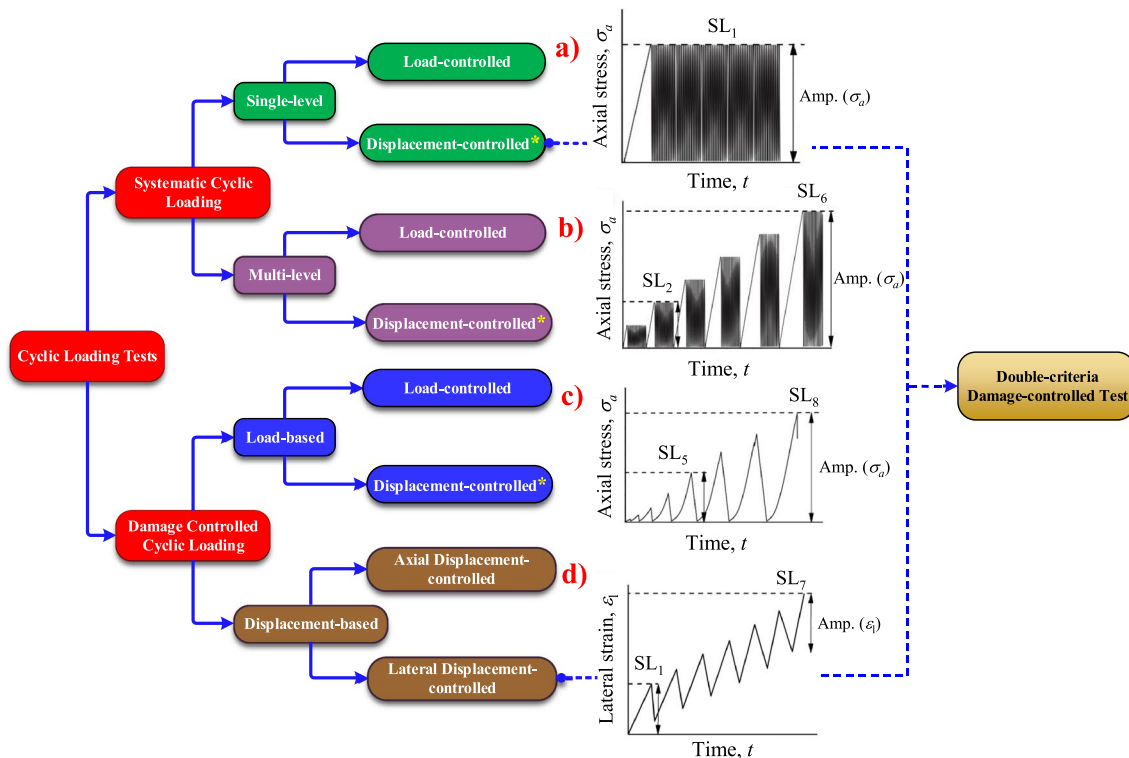
Fig. 2 Classification of cyclic loading tests, **a** single-level systematic cyclic loading path, **b** multi-level systematic cyclic loading path, **c** load-based damage controlled cyclic loading path and **d** displacement-based damage controlled cyclic loading path, Amp. (σ_a) refers to loading amplitude, Amp. ($\mathcal{E}_l$) refers to lateral strain amplitude, and * can be conducted either in axial or lateral displacement-controlled mode, modified from Shirani Faradonbeh et al. (2020)

failure occurs during cyclic loading as a constant axial load amplitude, Amp.(σ_a), should be achieved during each loading cycle (e.g. Ma et al. 2013; Li et al. 2019). Similarly, in the load-based damage-controlled cyclic loading tests, as the specimen is forced to reach a prescribed stress level, it may experience an unexpected failure, and the post-peak behaviour cannot be captured (e.g. Heap et al. 2010; Guo et al. 2018). Regarding the displacement-based damage-controlled cyclic loading tests, as the post-peak behaviour of rocks in uniaxial compression is either class II or a combination of classes I and II (Munoz et al. 2016a), the post-peak response cannot be adequately captured by the axial displacement feedback signal (e.g. Wang et al. 2019). The lateral displacement, on the other hand, has been identified as an appropriate variable to control the amount of damage in the post-peak regime (Munoz and Taheri 2019).

To our knowledge, no prior studies have examined the influence of systematic cyclic loading at different stress levels on the post-peak behaviour of rocks. This is due to the difficulties in controlling the axial load when a constant load amplitude should be achieved in every cycle in a systematic cyclic loading test. Also, if a prescribed lateral strain is considered to control the damage in a damage-controlled test, the axial load is reversed when a certain amount of lateral strain occurs, and therefore, the systematic cyclic loading cannot be conducted anymore in the pre-peak regime. However, as mentioned earlier, some mining and civil structures (e.g. mining pillars and bridge columns) may experience systematic cyclic loading at different fractions of their average peak strength. Under such loading conditions, the rocks may exhibit different behaviours in the post-peak regime. An appropriate experimental methodology is, therefore, required for measuring the post-peak behaviour of rocks subjected to systematic cyclic loading histories properly. As demonstrated in Fig. 2, a novel cyclic test method by combining the single-level systematic cyclic loading and lateral displacement-based damage-controlled cyclic loading is proposed in this study to control both the damage and the cyclic loading rate. Then, several systematic cyclic tests were conducted in uniaxial compression at different stress levels using the proposed test method. Based on the obtained complete stress–strain relations, the influence of systematic cyclic loading on both the pre-peak and the post-peak behaviours was evaluated comprehensively, and the results were discussed in detail.

2 Specimen Preparation and Experimental Set-Up

The Gosford sandstone as a medium-grained (0.2–0.3 mm), poorly cemented, immature quartz sandstone containing 20–30% feldspar and clay minerals with the serrate

connection between quartz grains (Sufian and Russell 2013) was used in this study for conducting the experimental tests. According to the X-ray computed tomography scans conducted by Sufian and Russell (2013), the total porosity of this sandstone is about 18%. A total of 23 cylindrical specimens having a constant aspect ratio of 2.4 (i.e. 42 mm diameter and 100 mm length) were all cored from the same rectangular block and in the same direction and prepared according to the ISRM suggested method (Fairhurst and Hudson 1999). In this study, all the experiments were performed in dry condition. To do so, the rock specimens were dried in room temperature before conducting the tests. The average dry density of the specimens was approximately 2204.26 kg/m^3. Rock monotonic strength should be determined before undertaking systematic cyclic loading tests at different stress levels (σ_a/σ_m). To do so, six uniaxial compression tests were performed following the lateral strain-controlled loading method. An MTS close-looped servo-controlled hydraulic compressive system having the maximum loading capacity of 300 kN (see Fig. 3) was used to undertake the monotonic and cyclic loading tests. As stated earlier, the axial load-controlled and axial strain-controlled loading techniques cannot capture the post-peak behaviour of rocks, as rocks usually show a combination of class I and class II behaviour in the post-peak regime (Munoz et al. 2016b). Therefore,
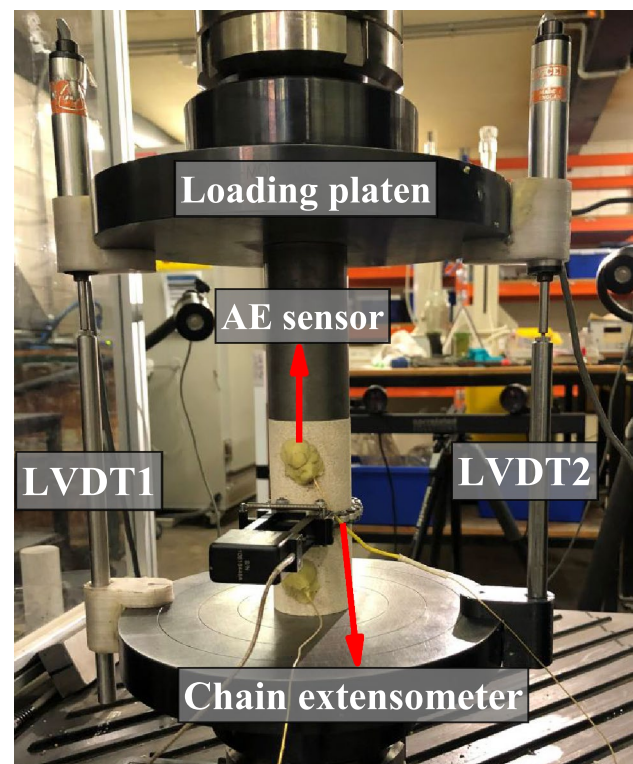
Fig. 3 Testing set-up for the uniaxial compression and cyclic loading tests

as depicted in Fig. 4a, a constant lateral strain rate $(d\varepsilon_l/d_t)$ of 0.02×10^{-4}/s was utilised during the uniaxial compression tests to control the axial load both in the pre-peak and the post-peak regimes. This strain rate provides a static to quasi-static loading conditions (Wawersik and Fairhurst 1970; Munoz et al. 2016b).

Axial load and axial and lateral displacements were recorded in real-time, respectively using the load cell, a pair of LVDTs externally mounted between the loading platens and a direct-contact chain extensometer wrapped around the specimens (see Fig. 3). Due to the large-strain behaviour of rocks in the post-peak regime, the local strain measurement tools such as strain gauges are not effective. To characterise the post-peak instability of rocks in terms of brittleness, the complete stress–strain curves of rocks are required, and therefore, external LVDTs were used to measure the large-strain properties. LVDTs measure the deformation between loading platens; therefore, the deformation of the loading system is not included in the measurement. Still, the strain
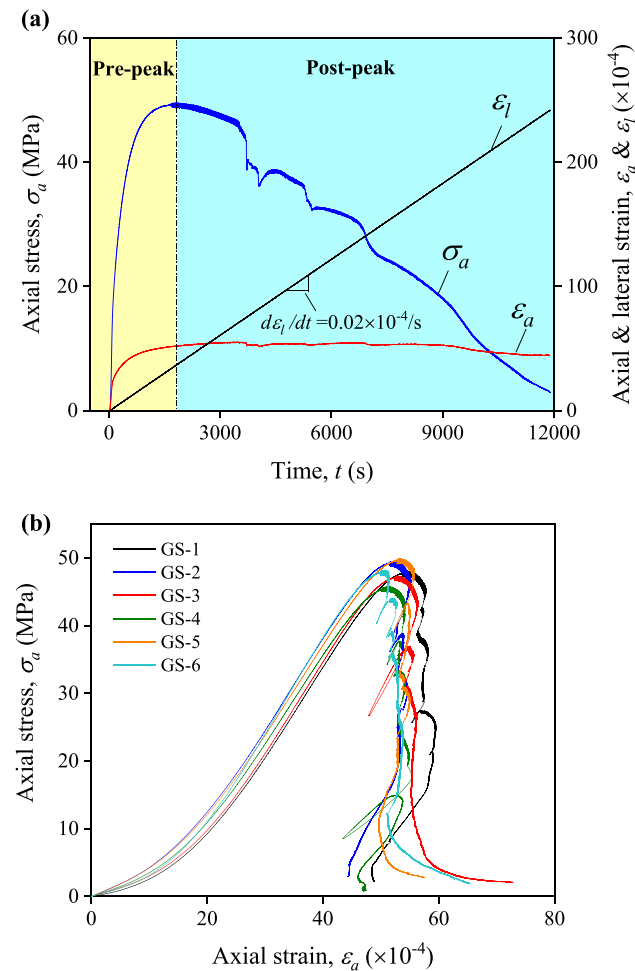
data may not be precise due to well-known bedding error (Taheri and Tani 2008). The bedding error refers to the additional deformations measured by LVDTs due to crushing the irregularities/asperities at the end faces of the specimens before the specimen deforms as well as the poor fitting of the specimen to the loading platens. This error is minimised in this study by carefully and smoothly grinding the ends of the specimen following the ISRM standard (Fairhurst and Hudson 1999). Besides, since the focus of this study is complete stress–strain behaviour, this error is deemed negligible in large strain stress–strain properties.

The acoustic emission (AE) technique, as a passive non-destructive monitoring technology, was also employed in this study to measure the real-time formation and growth of local micro-cracks throughout the specimen (internal damage) during cyclic loading (Lockner 1993; Bruning et al. 2018). For this aim, as depicted in Fig. 3, two miniature PICO sensors were attached to the specimens, and the recorded acoustic signals by these sensors were amplified using a pre-amplifier (type 2/4/6) set to 60 dB of gain. The AE recordings were carried out using the Express-8 data acquisition card with sampling rate of 2 MSPS (million samples per second). To ensure that mechanical noises induced by the loading system are not recorded during the tests, the AE threshold amplitude was changed from 20 to 60 dB, and it was found that after 45 dB amplitude, no additional noises are recorded. Therefore, this value was set as the AE threshold.

The stress–strain curves obtained from the conducted uniaxial compressive tests and their relevant mechanical properties can be found in Fig. 4b, and Table 1, respectively. In Table 1, the tangent Young's modulus (E_{tan}) and Poisson's ratio (v) values were determined at 50% of the axial peak stress (σ_{a-peak}) for each monotonic test. The crack initiation stress (σ_{ci}) and crack damage stress (σ_{cd}) thresholds were also determined using the methods explained in Taheri et al. (2020). According to Fig. 4b, the stress–strain curves for all compression tests show almost a similar behavioural trend both in the pre-peak and the post-peak regimes. In the pre-peak regime, as listed in Table 1, the deformation parameters of axial (ε_{a-peak}), lateral (ε_{l-peak}) and volumetric strains (ε_{v-peak}) at peak stress points, E_{tan}, v, crack initiation stress ratio ($\sigma_{ci}/\sigma_{a-peak}$) and crack damage stress ratio ($\sigma_{cd}/\sigma_{a-peak}$) are approximately similar, which indicates a small discreteness of the tested specimens. As such, in the post-failure regime, the sudden drops and recoveries of the load-bearing capacity can be observed for all specimens which can be associated with the shear strain localisation, grain interlocking in between the sides of the generated macrocracks (Jansen and Shah 1997; Vasconcelos et al. 2009) as well as the automatic adjustment of applied load by the testing machine upon damage extension. The post-peak regime of rocks under uniaxial compressive loading demonstrates

Fig. 4 **a** Typical time-history of the loading and strains during compressive tests and **b** axial stress–strain relations obtained from the monotonic loading tests

Table 1 The results of uniaxial compressive tests for Gosford sandstone specimens

Test no	$\sigma_{a-\text{peak}}$(MPa)	E_{tan} (GPa)	V	Strains at the peak stress point			$\sigma_{ci}/\sigma_{a-\text{peak}}$(%)	$\sigma_{cd}/\sigma_{a-peak}$(%)
				$\varepsilon_{a-\text{peak}}(\times 10^{-4})$	$\varepsilon_{l-\text{peak}}(\times 10^{-4})$	$\varepsilon_{v-\text{peak}}(\times 10^{-4})$		
GS-1	48.05	13.30	0.15	54.17	− 38.35	− 22.54	29.65	58.27
GS-2	49.54	13.43	0.12	52.18	− 36.84	− 21.51	30.60	58.67
GS-3	47.35	13.42	0.13	52.66	− 39.10	− 25.55	27.00	55.57
GS-4	45.76	12.97	0.15	51.39	− 38.56	− 25.73	25.80	55.96
GS-5	49.89	13.15	0.14	53.00	− 36.97	− 20.95	27.71	57.92
GS-6	48.29	14.14	0.15	50.17	− 34.11	− 18.05	26.94	52.70
Average	48.15	13.40	0.14	52.26	− 37.32	− 22.39	27.95	56.51
SD	1.51	0.40	0.01	1.38	1.81	2.93	1.82	2.25

SD standard deviation

a combined classes I–II behaviour, which is consistent with the prior study conducted by Munoz et al. (2016b). As listed in Table 1, the monotonic compressive strength ($\sigma_{a-\text{peak}}$) of the tested Gosford sandstone specimens varied between 45.76 and 49.89 MPa with an average value of 48.15 MPa. This average monotonic strength was utilised in the following to define the stress levels where the systematic cyclic loading tests should be commenced.

3 Systematic Cyclic Loading Tests

As discussed earlier, the single-criterion load-based and displacement-based loading methods are not sufficient to control the axial load in the post-failure stage during the systematic cyclic loading tests, especially when rocks demonstrate self-sustained failure behaviour. In this study, to address this issue, a new testing method called "double-criteria damage-controlled test method" (Shirani Faradonbeh et al. 2020) was employed. As demonstrated in Fig. 2, this test method is a combination of single-level systematic cyclic loading and damage-controlled cyclic loading lateral displacement-controlled loading method. In this regard, the MTS servo-controlled testing machine was programmed so that the hydraulic system was allowed to be adjusted continuously, automatically and rapidly according to the received feedback signals from both chain extensometer and load cell during a closed-loop procedure. The testing procedure can be summarised into the following four stages:

1. Load the specimen monotonically ($d\varepsilon_l/dt = 0.02 \times 10^{-4}$) until the pre-defined stress level (σ_a/σ_m), and then, unload it at the same loading rate until $\sigma_a = 0.07$ MPa, ensuring the specimen is always in complete contact with the loading platens.
2. Reload the specimen under a constant lateral strain rate of 3×10^{-4}/s until one of the two following criteria is met during loading:
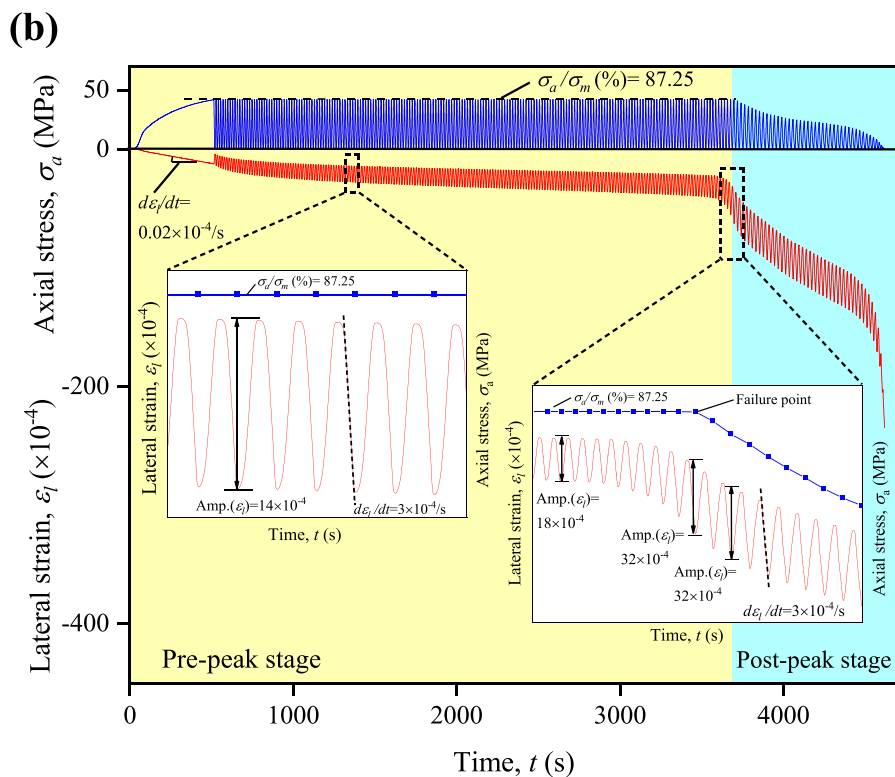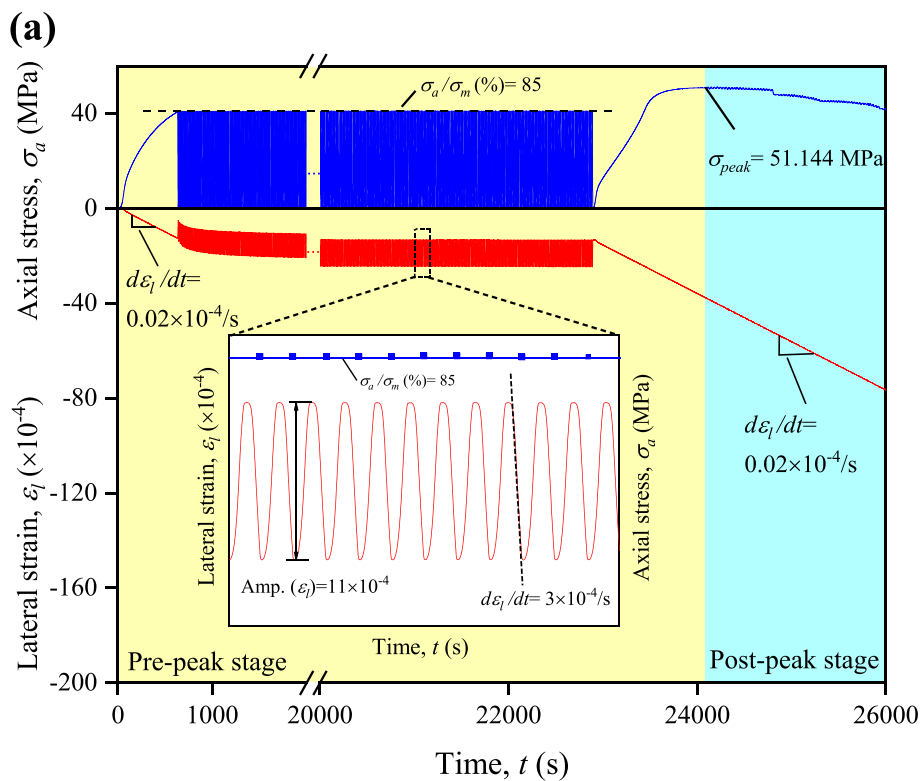
   (a) the pre-defined maximum axial stress level (σ_a/σ_m) is reached;
   (b) the pre-defined maximum lateral strain amplitude, Amp. $(\varepsilon_l) = 32 \times 10^{-4}$ is reached;

3. Reverse the axial load to $\sigma_a = 0.07$ MPa, and repeat steps 1 and 2 until 1500 loading and unloading cycles are completed.
4. If the specimen did no fail during 1500 cycles, apply a monotonic loading ($d\varepsilon_l/dt = 0.02 \times 10^{-4}$) until complete failure occurs.

In this study, Amp. $(\varepsilon_l) = 32 \times 10^{-4}$ was determined based on the conducted monotonic tests and the measured lateral strain of the rocks at the failure point, $\varepsilon_{l-\text{peak}}$ (see Table 1). As seen in Table 1, the average value of $\varepsilon_{l-\text{peak}}$ for the tested specimens is − 37.32×10^{-4}. Based on the conducted several trial tests, it was found that 32×10^{-4} is an appropriate value for Gosford sandstone. By adopting this value, it was possible to avoid failing the sample in a single cycle while allowing the axial stress level to reach the pre-defined value to apply a systematic cyclic loading.

Figure 5a, b show two representative time histories of axial stress and lateral strain for Gosford sandstone specimens experiencing failure during cyclic loading and final monotonic loading. In Fig. 5a, the specimen was loaded monotonically ($d\varepsilon_l/dt = 0.02 \times 10^{-4}$/s) up to 85% of the average monotonic strength ($\sigma_a/\sigma_m = 85\%$). Afterwards, the specimen was unloaded at the same rate, and then the systematic cyclic loading was initiated under the lateral strain rate of 3×10^{-4}/s. As shown in the inset figure, the cycles always met the first criterion (i.e. the maximum stress applied during a cycle remained constant) during the systematic cyclic loading and the Amp. (ε_l) was considerably lower than the pre-defined maximum amplitude for lateral strain (i.e. 32×10^{-4}) in each cycle. As during 1500 loading/unloading cycles, the Amp. (ε_l) did not exceed 32×10^{-4}, a monotonic loading was applied automatically

to the specimen under the lateral strain rate of 0.02×10^{-4}/s until the specimen is completely failed. By doing so, the post-peak behaviour was captured successfully for further

analyses. In Fig. 5b, the same cyclic loading procedure was applied to another specimen at a higher axial stress level (i.e. $\sigma_a/\sigma_m = 87.25\%$). In the pre-peak stage, the Amp. (ε_l)

increased gradually by increasing the cycle number, while the stress level was kept constant, satisfying the first criterion. However, at the onset of the failure (where the axial stress begins to reduce), the Amp. (ε_l) reached the predefined value of 32×10^{-4} (see the inset figure), and the second criterion was activated to control the cyclic loading. By transferring to the post-peak stage, and strength degradation, the subsequent cycles were carried out so that the Amp. (ε_l) was always constant until the complete failure of the specimen occurred. Following this test method, the rock specimen failed in a controlled way, and the post-peak behaviour was captured successfully.

4 Stress–Strain Relations

In total, 17 single-level systematic cyclic loading tests (see Table 2) were carried out at different stress levels (σ_a/σ_m) ranging from 80 to 96% of the average monotonic strength following the proposed double-criteria damage-controlled testing method. As listed in Table 1, the stable and unstable crack growths of rocks on average initiate at $\sigma_{ci}/\sigma_{a-\text{peak}} = 27.95\%$ and $\sigma_{cd}/\sigma_{a-\text{peak}} = 56.51\%$, respectively. This, in other words, shows that the cyclic loading tests have been conducted in the unstable crack propagation stage, beyond the elastic stress–strain behaviour. To evaluate the influence of cycle number on mechanical properties and post-peak behaviour, the specimens GS-8 and GS-9 were subjected to 5000 and 10,000 cycles at $\sigma_a/\sigma_m = 80\%$

and GS-11 experienced 5000 cycles at the stress level of $\sigma_a/\sigma_m = 85\%$ before a monotonic loading. Otherwise, the samples experienced a maximum of 1500 cycles and then a post-monotonic loading should they did not fail during the cyclic loading. According to Beniawski (1967), to ensure fatigue failure of a rock specimen in a timely manner, the cyclic loading test should be conducted just before the onset of the unstable crack propagation stage within the range of 70–85% of the peak strength. A recent review conducted by Cerfontaine and Collin (2018) on rock fatigue studies reported that the rock fatigue threshold ranges from 0.75 to 0.9 of the average monotonic strength for one million loading and unloading cycles depending on rock type and loading conditions. However, in this study, due to test limitations, further cycles did not apply, and the results are valid in the range of 1500–10,000 cycles. Based on the results presented in Table 2, it is hypothesised that there exists a threshold of σ_a/σ_m which lies between 86 and 87.5% that indicates the critical boundary of rock strength hardening and fatigue under cyclic loading. In this study, the cyclic loading tests which experienced the monotonic loading at the failure stage were named as hardening cyclic loading tests, while those which failed during cyclic loading at higher stress levels were named as fatigue cyclic loading tests.

Figures 6 and 7 show the typical stress–strain results for hardening and fatigue cyclic loading tests, respectively. In these figures, the total post-peak behaviour was highlighted by connecting the indicator stresses (σ_i, the maximum stress of each cycle). The $\varepsilon_a^{\text{irr}}$ and $\varepsilon_l^{\text{irr}}$ respectively, represent the

Table 2 The results of the conducted systematic cyclic tests

Test no	σ_a/σ_m(%)	N_{total}	N_{after}	Hardening (H) or fatigue (F) test?	$\varepsilon_{a-f}(\times 10^{-4})$	$\varepsilon_{a-peak}(\times 10^{-4})$	Peak strength increase (%)
GS-7	80	1500	–	H	45.80	53.56	0.53
GS-8	80	5000	–	H	43.03	52.36	7.31
GS-9	80	10,000	–	H	48.94	55.98	0.05
GS-10	85	1500	–	H	46.38	53.70	6.22
GS-11	85	5000	–	H	48.93	54.29	2.17
GS-12	86	1500	–	H	45.52	50.92	1.93
GS-13	87.50	1500	–	H	47.72	55.04	7.82
GS-14	86.81	636	49	F	–	56.15	–
GS-15	87.23	49	26	F	–	56.06	–
GS-16	87.25	240	42	F	–	54.78	–
GS-17	89.65	40	28	F	–	54.75	–
GS-18	89.82	103	45	F	–	53.12	–
GS-19	91.76	145	97	F	–	52.75	–
GS-20	93	49	36	F	–	54.37	–
GS-21	93.65	280	260	F	–	54.98	–
GS-22	95	752	730	F	–	54.46	–
GS-23	96	474	318	F	–	37.84	–

N_{total} total number of cycles, N_{after} number of cycles after failure point, ε_{a-f} axial strain at the peak of the final cycle, $\varepsilon_{a-\text{peak}}$ axial strain at the failure point
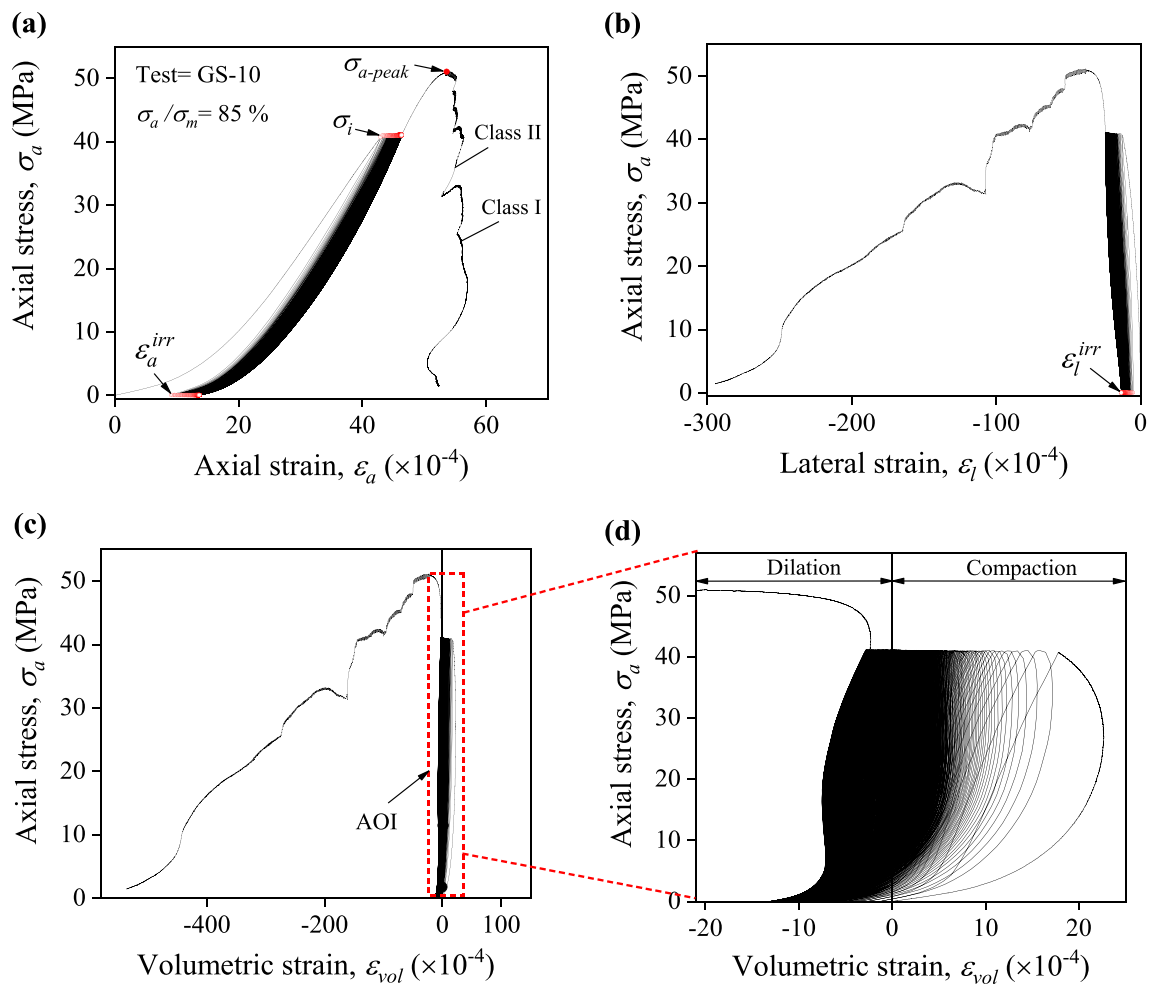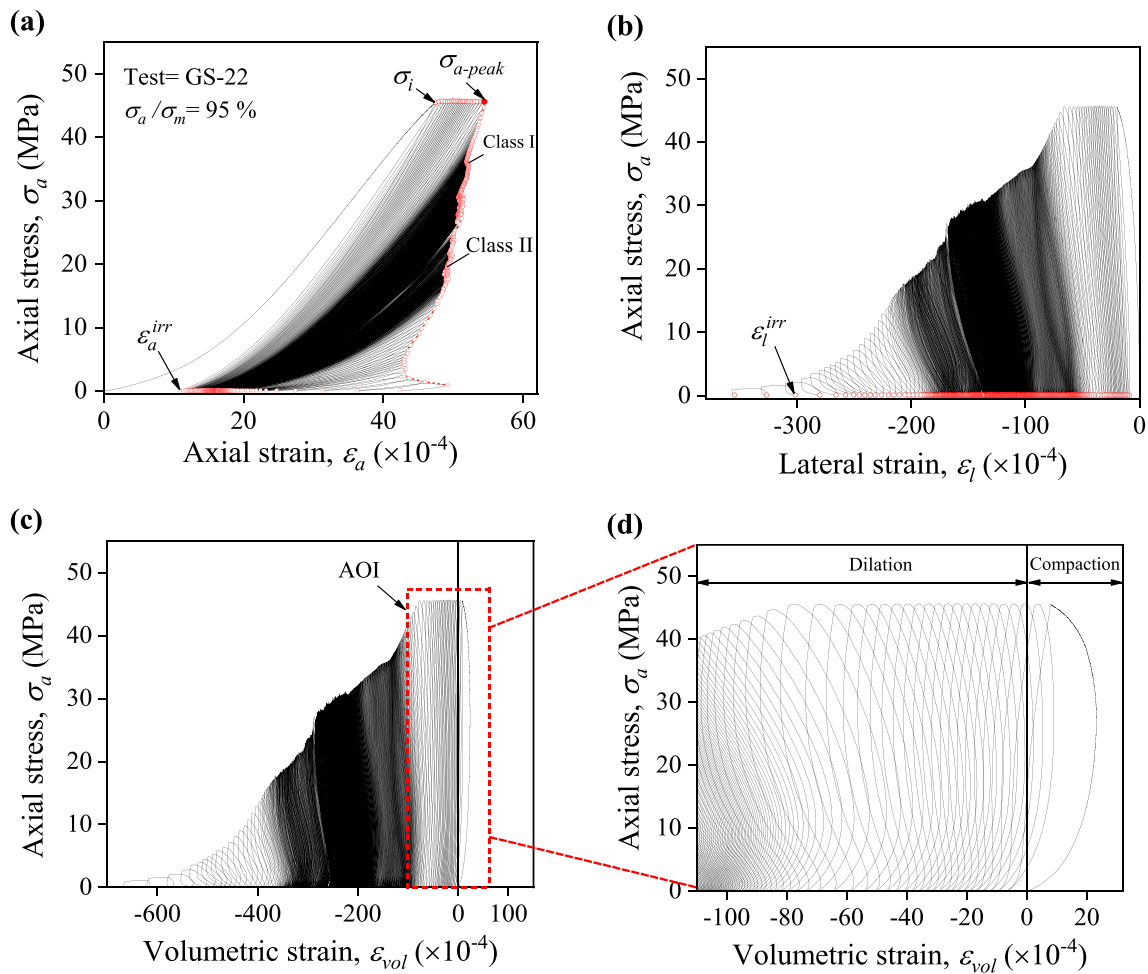
Fig. 6 Typical stress–strain results for the hardening cyclic loading tests (test GS-10)

irreversible axial strain and the irreversible lateral strain. The areas of interest (AOIs) shown in Figs. 6c and 7c illustrate the specific parts of the volumetric strain (ε_{vol}) evolution which were enlarged in Figs. 6d and 7d, respectively. Figures 6a and 7a show that the testing methodology was successful in capturing the complete stress–strain curves of Gosford sandstone specimens subjected to systematic cyclic loading. Furthermore, like the monotonic tests, a combined class I-II behaviour at different extents can be seen in the post-peak regime for both hardening and fatigue cyclic loading tests. Generally, the variation of hysteretic loops along with the axial strain (Figs. 6a, 7a), lateral strain (Figs. 6b, 7b) and volumetric strain (Figs. 6c, d and 7c, d) show that the rock specimens which fail during the cyclic loading significantly experience more irreversible strains in the pre-peak regime compared with hardening cyclic loading tests. In addition, as shown in Fig. 7d, after a few cycles, the hysteretic loops for the fatigue cyclic loading tests switch rapidly from the compaction to dilation, and dilation continues until complete failure.

5 Rock Behaviour During Hardening Cyclic Loading Tests

5.1 Damage Evolution in the Pre-Peak Regime

In rock engineering applications, the rock deformation and failure processes are associated with the strain energy evolution (Li et al. 2019). The total inputted mechanical energy during a loading and unloading cycle is transformed into the stored elastic energy (U_e^i) and the dissipated energy (U_d^i) as shown schematically in Fig. 8a. The dissipated energy due to the irreversible deformations causes stiffness degradation and rock damage. In this study, the energy dissipation ratio (i.e. $K = U_d/U_e$) and tangent Young's modulus ($E_{\tan}$) were utilised to investigate progressive damage evolution in the pre-peak regime for hardening cyclic loading tests. Figure 8b shows the representative results for specimen GS-10 at $\sigma_a/\sigma_m = 85\%$. The other hardening cyclic loading tests conducted at different stress levels and with a different number of cycles also showed a similar trend. According to Fig. 8b,

Fig. 7 Typical stress–strain results for the fatigue cyclic loading tests (test GS-22)

a two-stage damage evolution procedure can be identified for the hardening cyclic loading tests. In stage A, the E_{tan} increased dramatically during initial cycles (approximately 21.94% compared with the average E_{tan} for monotonic tests in Table 1), which can cause to specimen become stiffer. This behaviour can be relevant to the closure of existing defects. An increase of stiffness during the initial loading cycle also has been reported by other researchers (Trippetta et al. 2013; Momeni et al. 2015; Taheri and Tatsuoka 2015; Taheri et al. 2016b). On the other hand, the energy dissipation ratio (K) decreased suddenly in stage A, which contributes to the accumulation of elastic strain energy in rock specimen. In stage B, while it was expected to see stiffness degradation due to incurring irreversible deformations in the specimen by doing more cycles, E_{tan} and K remained fairly constant, and no considerable energy was dissipated until 1500 cycles were completed (i.e. a quasi-elastic behaviour).

This quasi-elastic behaviour can be further investigated using AE results. Figure 8c shows the typical time history of AE hits recorded for the specimen GS-10. As shown in

this figure, few AE hits are observed at the initial monotonic loading stage, which corresponds to seating, loading adjustment by the testing apparatus and the crack closure stage. However, in the second stage, almost no macrocrack (macro-damage) is generated throughout the specimen as a constant trend was observed for the cumulative AE hits during the 1500 cycles. In other words, at this stage, only small amounts of low amplitude AE hits (micro-damages) are generated (see Fig. 8c). During the final monotonic loading stage, new microcracks are generated and propagated throughout the specimen, and the cumulative AE hits increase gradually until the peak strength point. This is followed by the rapid rise of cumulative AE hits in the post-peak regime, where the microcracks coalesce, and the cohesive strength of the rock specimen degrades. On the other hand, according to Fig. 6, during hardening cyclic loading tests, the specimens do not experience large axial, lateral and volumetric irreversible deformations after 1500 cycles and the hysteretic loops for such tests are very dense. This clearly can be seen from the variation of volumetric strains in the area of interest
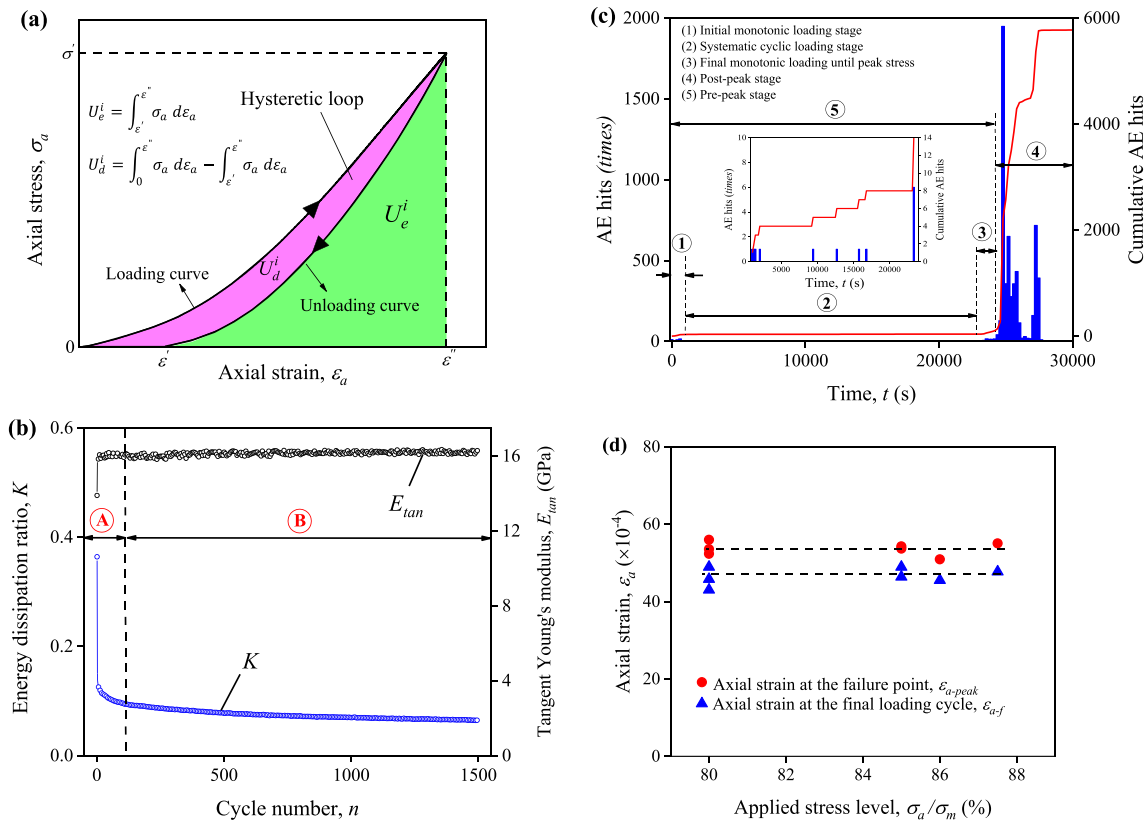
Fig. 8 **a** Energy components for a loading and unloading cycle, **b** typical evolution of the energy dissipation ratio and stiffness parameters for the specimen GS-10, **c** typical time-history of AE hits for the specimen GS-10, **d** the variation of axial strain at the final loading cycle and the failure point with stress level for hardening cyclic loading tests

(AOI) (see Fig. 6d). In Fig. 6d, it is observed that the slope of the hysteretic loops between the lowest points and the peak points is positive, implying that the current volume of the specimen is mostly at the compaction stage with slight dilation at the end of pre-peak cyclic loading. According to the evolution of damage parameters (i.e. E_{tan} and K), AE hits and the irreversible strains discussed above, the following potential mechanism can be inferred for the observed quasi-elastic behaviour in this study:
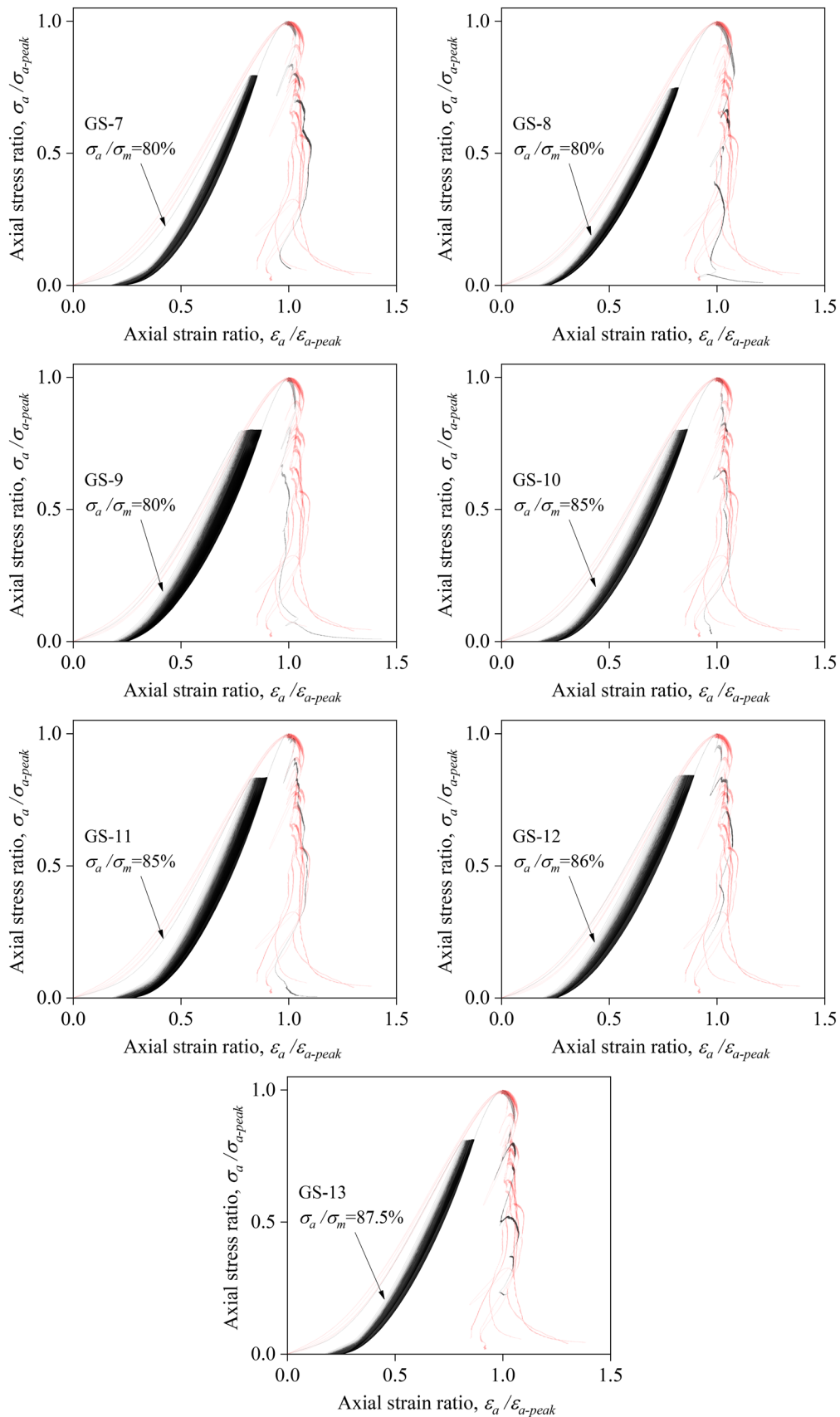
During cyclic loading below the fatigue threshold stress, but in the unstable crack propagation stage, some microcracks might be created within the specimens, which may result in grain size reduction and the creation of some pore spaces. The grain size reduction induced by cyclic loading also has been reported by Trippetta et al. (2013) based on the conducted microscopic analysis, although they used different loading history (i.e. damage-controlled cyclic loading tests). On the other hand, by performing additional loading and unloading cycles, the existing or newly generated defects which have been oriented horizontally are closed, and the rock specimen is compacted progressively. This is while the defects which have been oriented vertically are opened progressively. Therefore, it can be hypothesised that

the observed quasi-elastic behaviour in this study can be due to the competition between two mechanisms of dilatant microcracking, which degrades rock stiffness, and rock compaction, which increases stiffness.
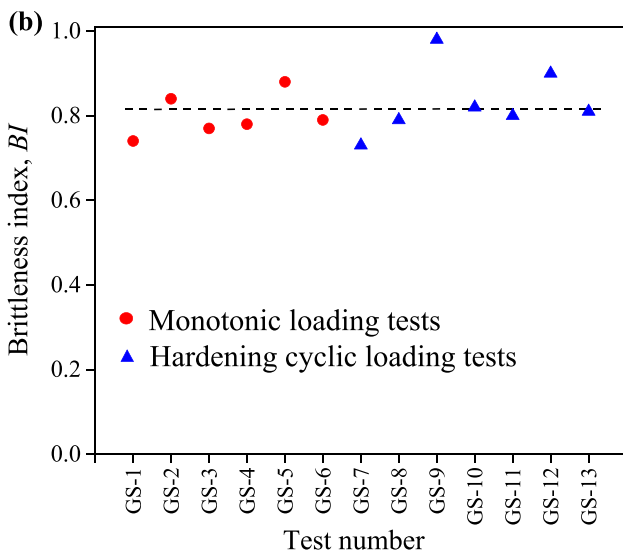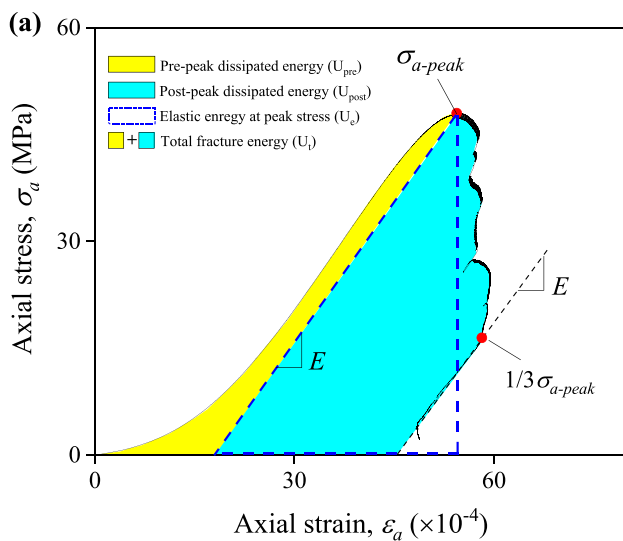
The damage evolution seems to be independent of the applied stress level as the same trends of K and E_{tan} and AE hits were observed for all hardening cyclic loading tests at different stress levels. This also can be proved by investigating the variation of axial strains at the final loading cycle (ε_{a-f}) and failure point ($\varepsilon_{a-\text{peak}}$) for hardening cyclic loading tests (see Table 2). As depicted in Fig. 8d, the variation of ε_{a-f} and $\varepsilon_{a-\text{peak}}$ with stress level is almost similar and constant for all hardening tests, which demonstrates the analogous damage evolution process.

5.2 Effect of Pre-Peak Cyclic Loading on the Post-Peak Monotonic Behaviour

In Fig. 9, the results of hardening cyclic loading tests are compared with monotonic test results, as normalised axial stress–strain curves. As it may be seen in this figure, the overall post-peak behaviour of monotonic and hardening cyclic loading tests are almost similar. Also, the increase

Fig. 9 Normalised axial stress–strain relations of hardening cyclic loading and monotonic tests

Fig. 10 **a** Strain energy components for monotonic loading and **b** brittleness index (*BI*) variation for monotonic loading and hardening cyclic loading tests

indices have been developed by different researchers; however, the strain energy-based indices perform relatively better than others (Zhang et al. 2016). The brittle vs. ductile behaviour of rock materials can be revealed in stress–strain curves during loading and failure. Thus, the rock brittleness indices, which consider the complete stress–strain behaviour of rocks may be more reliable. Munoz et al. (2016a) proposed three fracture energy-based brittleness indices considering both pre-peak and post-peak regimes of stress–strain curves for different rocks under uniaxial compressive tests. They reported that the proposed indices properly describe an unambiguous and monotonic scale of brittleness with increasing pre-peak strength parameters (i.e. σ_{cd}, E_{tan} and $\varepsilon_{a-\text{peak}}$). Therefore, in this study, the following equations were used to measure the overall brittleness (BI) of the tested specimens under systematic cyclic loading:

$$\text{BI} = \frac{U_e}{U_t} = \frac{U_e}{U_{\text{pre}} + U_{\text{post}}}, \tag{1}$$

$$U_e = \frac{\sigma_{a-\text{peak}}^2}{2E_{\text{tan}}}, \tag{2}$$

where U_t, U_e, U_{pre} and U_{post} are total fracture energy in the pre-peak and post-peak stages, elastic energy at peak stress, the pre-peak dissipated energy and the post-peak dissipated energy, respectively.

Figure 10a shows the different strain energy components defined above for rock brittleness determination under monotonic loading. For hardening cyclic loading tests (i.e. GS-7 to GS-13), the final monotonic loading stress–strain curves were extracted from the stress–strain relations shown in Fig. 9. The strain energy components were calculated for all monotonic and hardening cyclic loading tests, and the corresponding BI. values were determined. The results are listed in Table 3. Figure 10b shows the variation of *BI* values for these tests. As may be seen in this figure, the BI values of the specimens tested under hardening cyclic loading are almost similar to those obtained under the monotonic loading conditions. Therefore, it can betated that the pre-peak systematic cyclic loading, does not have a notable influence on the post-peak instability of rocks if it does not lead to failure.

5.3 Rock Strength Improvement

In this study, as listed in Table 2, the strength hardening percentage varied between 0.05 and 7.82% for the tested Gosford sandstone specimens. Figure 11a shows the variation of axial peak stress ($\sigma_{a-\text{peak}}$) for all monotonic and hardening cyclic loading tests. As demonstrated in this

in cycle number at stress levels $\sigma_a/\sigma_m = 80\%$ (from 1500 to 10,000 cycles) and $\sigma_a/\sigma_m = 85\%$ (from 1500 to 5000 cycles), has no significant influence on the general post-peak behaviour. In other words, when the stress level that cyclic loading is applied is not high enough to fail the specimen during cyclic loading, the cyclic loading has a negligible effect on the post-failure behaviour. This can be further investigated based on the variation of rock brittleness. Although there is no consensus regarding the rock brittleness definition and its criterion, it is well-known that brittle rocks show small irreversible deformation before peak strength which is followed by a self-sustaining failure in the post-peak regime (Tarasov and Potvin 2013). From 1956 to date, many rock brittleness

Table 3 The values of strain energy components and BI for different tests

Test type	Test no	U_{pre} (MPa)	U_e (MPa)	U_{post} (MPa)	U_{total} (MPa)	BI
Monotonic	GS-1	0.021	0.087	0.096	0.117	0.74
	GS-2	0.023	0.091	0.086	0.109	0.84
	GS-3	0.020	0.084	0.088	0.108	0.77
	GS-4	0.021	0.081	0.082	0.103	0.78
	GS-5	0.021	0.095	0.086	0.107	0.88
	GS-6	0.019	0.082	0.086	0.105	0.78
Hardening	GS-7	0.015	0.067	0.078	0.092	0.73
	GS-8	0.017	0.074	0.078	0.094	0.79
	GS-9	0.010	0.073	0.064	0.074	0.98
	GS-10	0.013	0.075	0.079	0.091	0.82
	GS-11	0.008	0.069	0.078	0.085	0.80
	GS-12	0.008	0.071	0.071	0.079	0.90
	GS-13	0.013	0.077	0.082	0.096	0.81
Fatigue	GS-14	0.042	0.064	0.058	0.100	0.64
	GS-15	0.025	0.066	0.067	0.091	0.73
	GS-16	0.029	0.065	0.064	0.094	0.70
	GS-17	0.023	0.068	0.067	0.090	0.76
	GS-18	0.026	0.067	0.081	0.107	0.62
	GS-19	0.042	0.068	0.058	0.099	0.69
	GS-20	0.038	0.076	0.049	0.087	0.87
	GS-21	0.041	0.073	0.055	0.096	0.76
	GS-22	0.040	0.076	0.049	0.089	0.85
	GS-23	0.021	0.061	0.051	0.072	0.85

figure, in general, higher σ_{a-peak} values are recorded for the specimens which experienced a cyclic loading history (i.e. hardening tests), and about half of the hardening cyclic loading tests have σ_{a-peak} values greater than the upper limit of the monotonic tests. Figure 11b shows the variation of the strength hardening ratio (σ_h/σ_m) against the applied stress level. According to this figure, the strength hardening seems to be independent of the applied stress level (σ_a/σ_m). As discussed in Sect. 5.1, after an initial stiffness improvement of the specimens for several cycles, a quasi-elastic behaviour dominated the damage evolution during the pre-peak cyclic loading. This behaviour was accompanied by progressive rock compaction (see Fig. 6) and strength improvement up to 8%. It should be noted that rock strength improvement induced by cyclic loading also has been reported in several

studies for porous Hawkesbury sandstone (up to 11%) (Taheri et al. 2016a, 2017), hard graywacke sandstone (up to 29%) (Singh 1989) and rock salt (up to 171%) (Ma et al. 2013). This shows that rocks depending on their intrinsic characteristics and the applied loading history and loading conditions, may show strength hardening behaviour at different extents. Taheri et al. (2017) argue that when the rock specimen is subjected to cyclic loading at a stress level lower than a threshold value, the weak bonding between the mesoscopic elements may be broken down, and the created fine materials, may fill up the internal voids, causing rock compaction and strength improvement.

It should be mentioned that other potential mechanisms such as microcrack tip blunting and the interlocking of grains/asperities may involve strength hardening. For
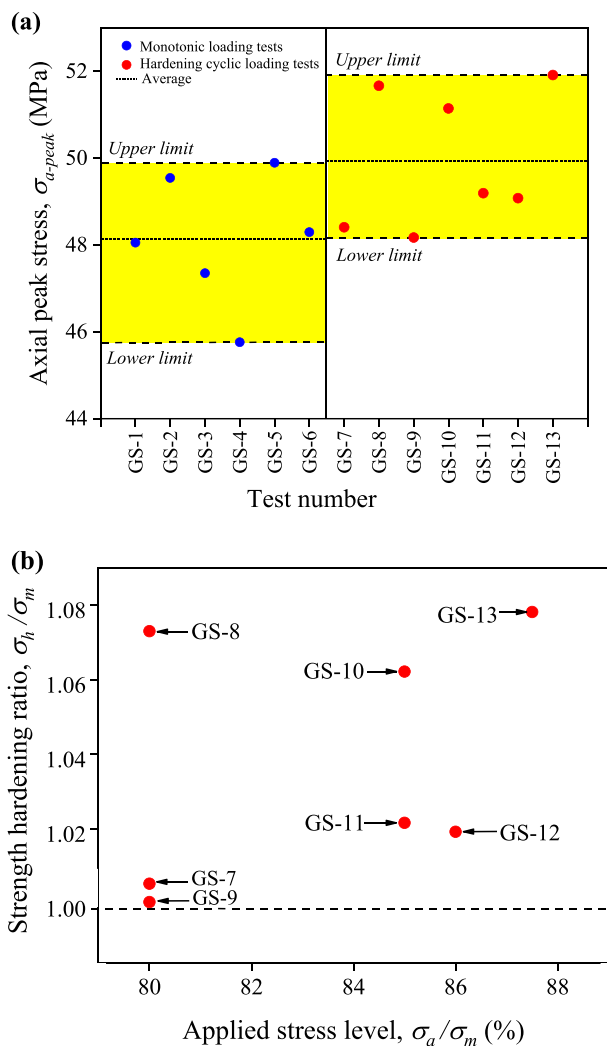
Fig. 11 a The variation of axial peak stress for all monotonic and hardening cyclic loading tests and **b** strength hardening ratio vs. applied stress level for hardening cyclic loading tests

instance, by considering the initial porosity of Gosford sandstone (i.e. 18%), due to the grain size reduction induced by cyclic loading during the quasi-elastic stage, some additional pore spaces might be generated within the specimens. When the cyclic loading-induced microcracks meet these pores, their tips may become blunt, resulting in a decrease in stress concentration at the crack tips and an increase in fracture

toughness. This, on the other hand, may cause to stopping the microcrack propagation. This behaviour can also be accompanied by grain interlocking, closure of cracks, and finally, compaction of the specimens during cyclic loading. Further microscopic investigations will shed more light on the cyclic loading-induced hardening mechanism.

6 Rock Behaviour During Fatigue Cyclic Loading Tests

6.1 Evaluation of Post-Peak Behaviour

As discussed in Sect. 5.2, the systematic cyclic loading has no notable effect on the post-peak behaviour of Gosford sandstone specimens if the cyclic stress level is below fatigue threshold stress. In this section, the influence of systematic cyclic loading beyond the fatigue threshold stress on the post-peak behaviour of Gosford sandstone specimens was evaluated. Figure 12 shows the normalised axial stress–strain curves for both monotonic tests and fatigue cyclic loading tests. The effect of cyclic loading history on the post-failure behaviour can be evaluated using the variation of rock brittleness index (BI) with the applied stress level. To do so, the envelope curve connecting the loci of the indicator stresses (σ_i) both in the pre-peak and the post-peak regimes were drawn, and the same procedure explained in Sect. 5.2 was utilised to measure the overall brittleness index. Figure 13a shows the extracted envelope curve for the typical test of GS-16. The strain energy components along with the BI values were determined for all fatigue cyclic loading tests, and the obtained values were tabulated in Table 3. Figure 13b displays the variation of BI values with the applied stress level. From this figure, it can be observed that the overall rock brittleness increases with an increase in the applied stress level. This means that rock may fail in a more brittle manner when it experiences cyclic loading at the stress levels close to its monotonic strength. In other words, in deep underground excavations, a cyclic loading history induced by seismic events that exceed the fatigue threshold stress may result in more violent failure causing casualties and financial loss. On the other hand, the weak seismic events which are applied at stress levels much lower than the rock monotonic strength do not seem critical
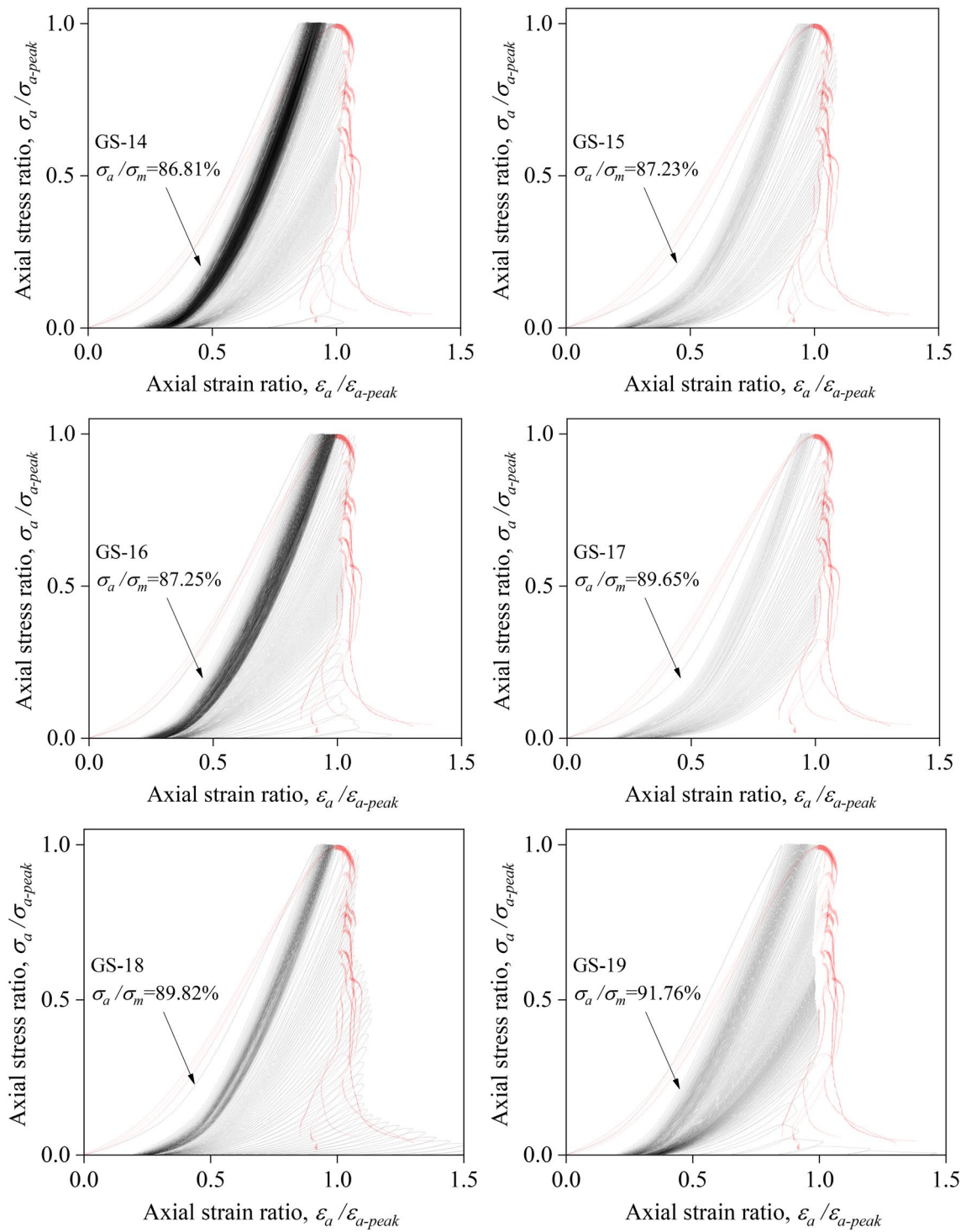
Fig. 12 Normalised axial stress–strain relations of fatigue cyclic loading and monotonic tests
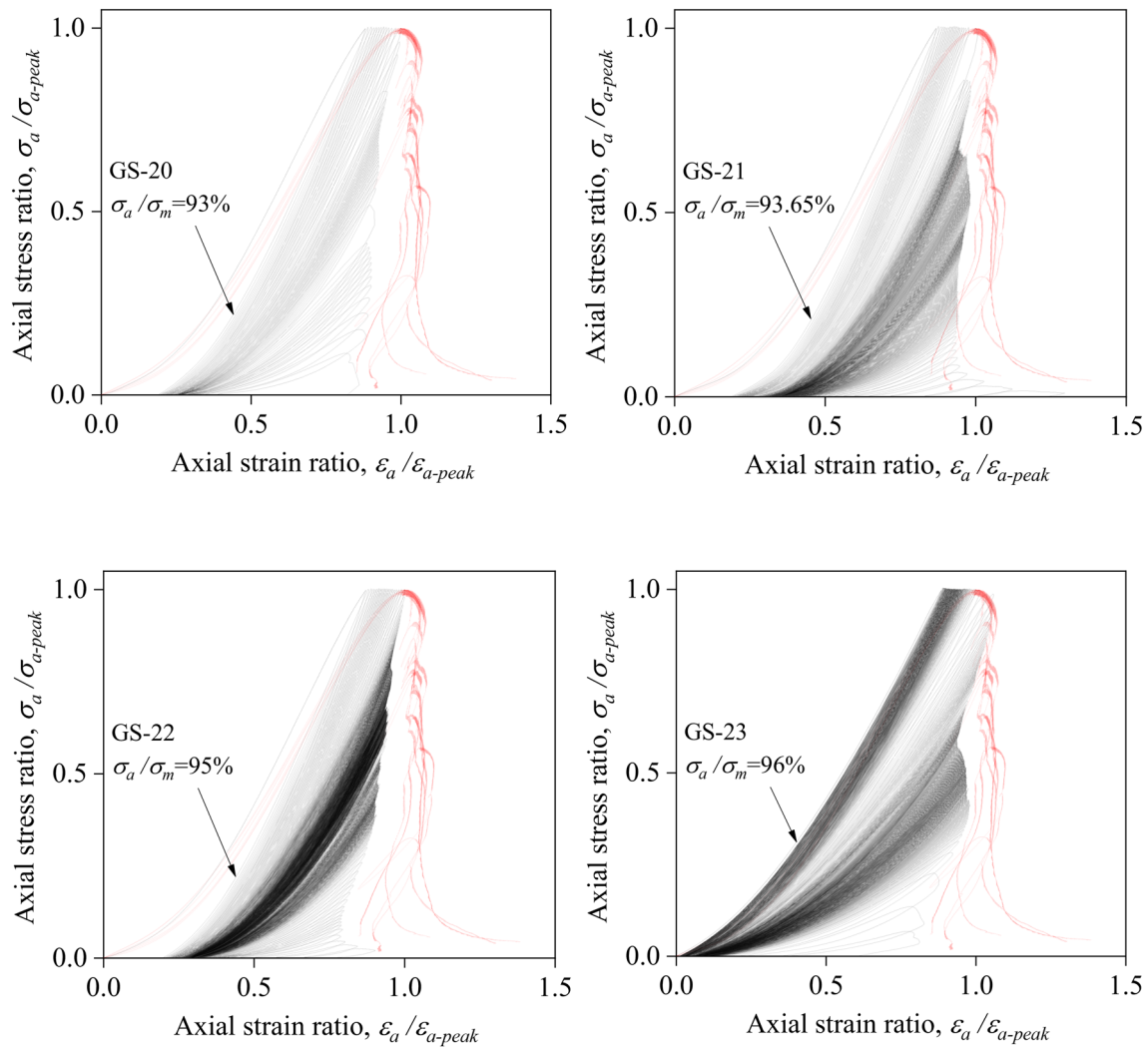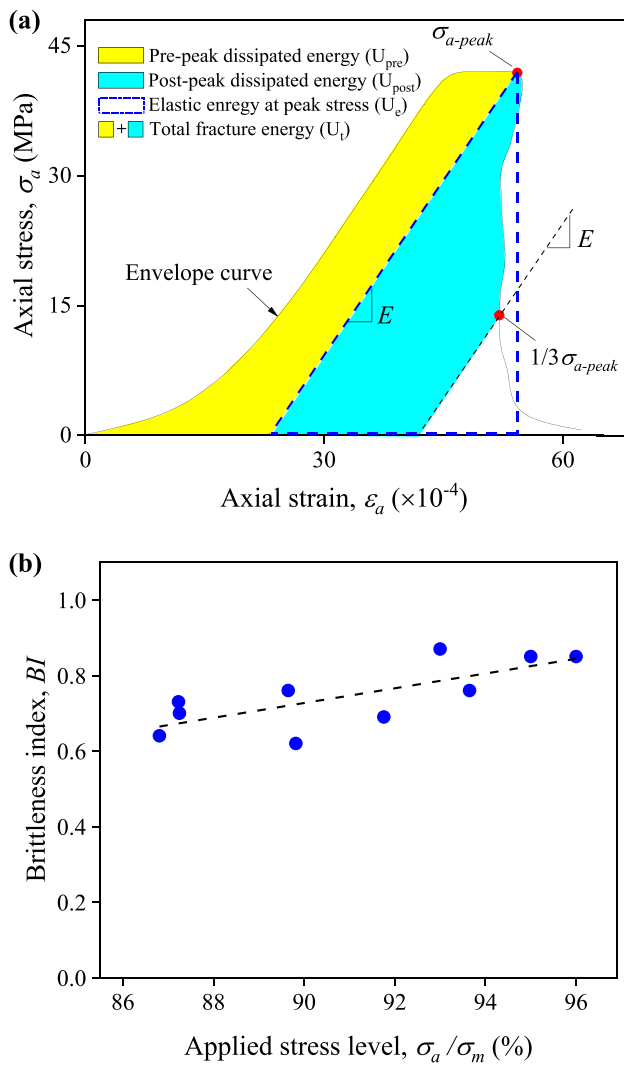
Fig. 12 (continued)

to damage the structures. These seismic events may even, slightly improve long-term stability.

6.2 Damage Evolution in the Post-Peak Regime

The irreversible deformations are not accumulated at a constant rate in the rock specimen during the pre-peak cyclic loading but follow an inverted S-shaped behaviour comprising three main phases of transient, steady and acceleration (Fig. 14a) (Royer-Carfagni and Salvatore 2000; Xiao et al. 2009; Fuenkajorn and Phueakphum 2010). These three phases are manifested as loose-dense-loose behaviour in the stress–strain curves of systematic cyclic loading based on the variation of hysteretic loops (Fig. 14b). According to Zoback and Byerlee (1975), the initial loose cycles correspond to the energy consumption for crack growth, that stabilises after several cycles. In the second phase that hysteric loops are closed and dense, the frictional work is more dominant, and the micro-cracks are opened and closed constantly without any significant extension. However, when the rock specimen is close to the failure point (i.e. the acceleration phase), the crack growth dominates, and hysteresis of the

pre-peak regime (Modified from Guo et al. 2012), **c**, **d** the loose-dense-loose behaviour in the post-peak regime of specimen GS-23, **e**, **f** the evolution of cumulative irreversible strains in the post-peak regime for specimen GS-23, **g** the secondary inverted S-shaped damage behaviour in the post-peak regime for specimen GS-23 and **h** the number of cycles after failure point versus the applied stress level for the fatigue cyclic loading tests

end of the pre-peak systematic cyclic loading extends to the post-peak regime and then accelerates. In Fig. 14e, f the cumulative irreversible axial ($\sum \varepsilon_a^{\mathrm{irr}}$) and cumulative irreversible lateral strains ($\sum \varepsilon_l^{irr}$) measured after full unloading of each loading cycle in the post-peak regime of specimen GS-23 are plotted against the axial stress ratio ($\sigma_a/\sigma_{a-\mathrm{peak}}$). According to these figures, when the specimen loses its load-bearing capacity until $\sigma_a/\sigma_{a-\mathrm{peak}} = 0.69$, due to quick dissipation of strain energy, the cumulative irreversible strains increases rapidly, which provided the loose hysteretic loops. Then, interestingly, the hysteretic loops are closed and experience a dense behaviour for a large number of cycles in the post-peak regime until $\sigma_a/\sigma_{a-\mathrm{peak}} = 0.38$. Finally, by the creation of large axial and lateral deformations within the specimen, the cumulative irreversible strains increased dramatically until complete failure occurred. This, in turn, provided the final loose hysteretic loops.

The observed loose-dense-loose behaviour in the post-peak regime for this specimen can be summarised as a secondary inverted S-shaped damage behaviour, as shown in Fig. 14g. Depending on the number of cycles that the specimens have experienced after the failure point, similar damage evolution trends with different extents also were observed for other fatigue cyclic loading tests. According to Table 2 and as shown in Fig. 14h, it can be observed that with the increase of applied stress level (σ_a/σ_m), the number of cycles after failure point increases exponentially, which is consistent with the formation of the secondary three-stage inverted S-shaped behaviour in the post-peak regime. In other words, it can be found out that the damage per loading/unloading cycle in the post-peak regime of the fatigue cyclic loading tests decreases with the increase of the applied stress level.

7 Conclusions

In this study, a series of systematic cyclic loading tests were conducted on Gosford sandstone specimens using an innovative double-criteria damage-controlled testing method. A comprehensive evaluation was carried out on the experimental results in terms of damage evolution, post-peak instability and strength hardening behaviour. The following conclusions can be drawn:

Fig. 13 **a** Strain energy components for the fatigue cyclic loading tests and **b** variation of brittleness index with the applied stress level for the fatigue cyclic loading tests

cycles increases. At higher stress levels, due to the rapid accumulation of damage, the steady phase will not be visible. On the other hand, at lower stress levels (as discussed in Sect. 5.1), after the initial phase, a steady-state dominates the whole test for a long time (Xiao et al. 2009).

According to the stress–strain curves obtained for the fatigue cyclic loading tests in this study (Fig. 11), the loose-dense-loose behaviour with different extents can be identified for hysteretic loops not only in the pre-peak regime but also in the post-peak regime. For instance, Fig. 14c, d shows the typical results for specimen GS-23 in which the loose-dense-loose behaviours are evident. As shown in the inset figure of the axial stress–strain curve, in the pre-peak regime, the hysteretic loops follow a loose-dense-loose behaviour according to the mechanism explained above. The loose behaviour at the
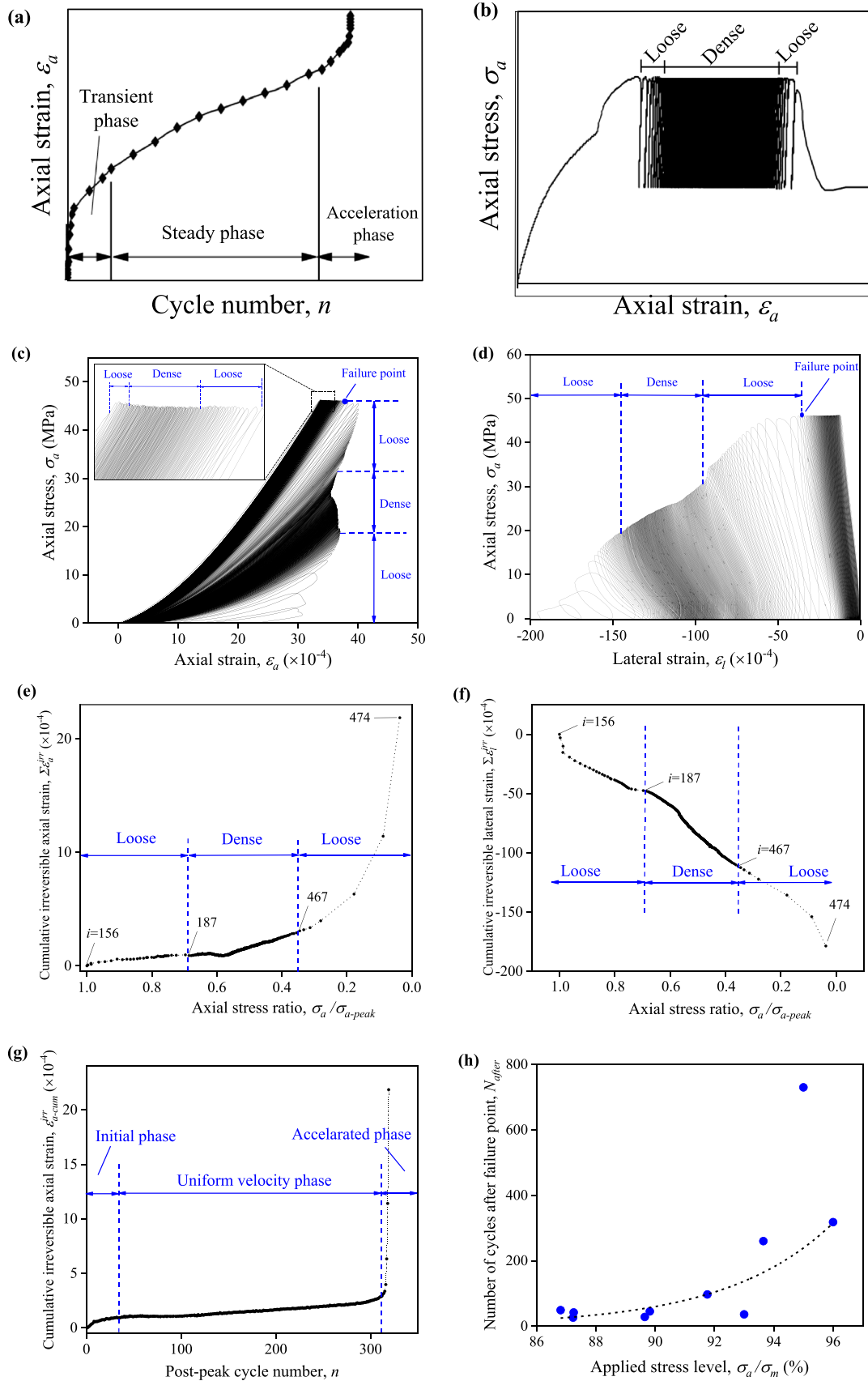
1. It was found that there exists a threshold of σ_a/σ_m, which lies between 86 and 87.5%. For σ_a/σ_m lower than this range, the specimens did not fail after experiencing a large number of cycles. The evaluation of the energy dissipation ratio, tangent Young's modulus and AE hits for hardening cyclic loading tests showed that the rock specimens follow a two-stage damage evolution law dominated by a quasi-elastic behaviour in the pre-peak regime. This quasi-elastic behaviour can be attributed to a balance between two mechanisms of dilatant microcracking and rock compaction during cyclic loading below the fatigue threshold stress. Moreover, the damage evolution in the pre-peak regime of the hardening cyclic loading tests was found to be independent of the number of cycles, as no significant influence on damage and/or hardening behaviour was observed by increasing the cycle number from 1500 to 10,000 cycles.

2. A similar pre-peak and post-peak behaviour was observed for monotonic tests and hardening cyclic loading tests when they were compared as the normalised axial stress–strain relations. Also, according to the variation of an energy-based brittleness index (BI), it was found that the pre-peak systematic cyclic loading has negligible influence on the post-failure instability when the applied stress level is not high enough to fail the specimen during cyclic loading.

3. For the specimens subjected to the systematic cyclic loading below the fatigue threshold stress, the peak strength increased up to 8% after applying the monotonic loading. This strength enhancement might be due to rock compaction and porosity reduction mechanism induced by cyclic loading. On the other hand, fatigue failure was observed for the specimens cyclically loaded beyond the fatigue threshold stress. For such tests, a rapid accumulation of lateral and volumetric strains was observed in the pre-peak regime.

4. For the systematic cyclic loading tests conducted beyond the fatigue threshold stress, it was observed that with the increase of the applied stress level, the rock specimens tend to behave as self-sustained in the post-failure stage. This was confirmed by the increase of brittleness index (BI) with σ_a/σ_m for the fatigue cyclic loading tests. Therefore, rocks may behave in a more brittle/violent manner when the cyclic loading is applied at stress levels close to their monotonic strength.

5. The evolution of hysteretic loops for fatigue cyclic loading tests showed that the rock specimens follow a loose-dense-loose behaviour in the pre-peak regime. However, the loose behaviour before the failure point is extended to the post-peak stage for several cycles. These loose hysteretic loops are followed by a dense behaviour for a large number of cycles until the complete failure of the specimen occurs, demonstrating another loose behav-

iour. This generally can be manifested as a secondary inverted non-linear S-shaped damage behaviour when the cumulative axial and cumulative lateral irreversible strains are plotted against the post-peak cycle number. It was observed that damage per cycle decreases exponentially with the increase of the applied stress level, and the three phases of the inverted S-shaped damage behaviour become more visible in the post-peak regime.

Declarations

References

Beniawski ZT (1967) Mechanism of brittle fracture of rock: part I—theory of the fracture process. Int J Rock Mech Min Sci 4(4):395–406

Bruning T, Karakus M, Nguyen GD, Goodchild D (2018) Experimental study on the damage evolution of brittle rock under triaxial confinement with full circumferential train control. Rock Mech Rock Eng 51(11):3321–3341

Cardani G, Meda A (2004) Marble behaviour under monotonic and cyclic loading in tension. Constr Build Mater 18(6):419–424

Cattaneo S, Labuz JF (2001) Damage of marble from cyclic loading. J Mater Civ Eng 13(6):459–465

Cerfontaine B, Collin F (2018) Cyclic and fatigue behaviour of rock materials: review, interpretation and research perspectives. Rock Mech Rock Eng 51(2):391–414

Erarslan N, Alehossein H, Williams DJ (2014) Tensile fracture strength of brisbane tuff by static and cyclic loading tests. Rock Mech Rock Eng 47(4):1135–1151

Fairhurst CE, Hudson JA (1999) Draft ISRM suggested method for the complete stress-strain curve for intact rock in uniaxial compression. Int J Rock Mech Min Sci 36(3):279–289

Fuenkajorn K, Phueakphum D (2010) Effects of cyclic loading on mechanical properties of Maha Sarakham salt. Eng Geol 112(1–4):43–52

Gong QM, Yin LJ, Wu SY et al (2012) Rock burst and slabbing failure and its influence on TBM excavation at headrace tunnels in Jinping II hydropower station. Eng Geol 124:98–108

Guo H, Ji M, Zhang Y, Zhang M (2018) Study of mechanical property of rock under uniaxial cyclic loading and unloading. Advances in Civil Engineering 2018, pp 1–6

Haimson BC (1978) Effect of cyclic loading on rock. In: Silver ML, Tiedemann D (eds) Dynamic geotechnical testing. ASTM International, West Conshohocken, pp 228–245

Heap MJ, Faulkner DR (2008) Quantifying the evolution of static elastic properties as crystalline rock approaches failure. Int J Rock Mech Min Sci 45(4):564–573

Heap MJ, Vinciguerra S, Meredith PG (2009) The evolution of elastic moduli with increasing crack damage during cyclic stressing of a basalt from Mt. Etna Volcano. Tectonophys 471(1):153–160

Heap MJ, Faulkner DR, Meredith PG, Vinciguerra S (2010) Elastic moduli evolution and accompanying stress changes with increasing crack damage: implications for stress changes around fault zones and volcanoes during deformation. Geophys J Int 183(1):225–236

Jansen D, Shah S (1997) Effect of length on compressive strain softening of concrete. J Eng Mech 123(1):25–35

Li T, Pei X, Wang D et al (2019) Nonlinear behavior and damage model for fractured rock under cyclic loading based on energy dissipation principle. Eng Fract Mech 206:330–341

Liu J, Xie H, Hou Z et al (2014) Damage evolution of rock salt under cyclic loading in unixial tests. Acta Geotech 9(1):153–160

Liu Q, Huang S, Kang Y, Liu X (2015) A prediction model for uniaxial compressive strength of deteriorated rocks due to freeze-thaw. Cold Reg Sci Technol 120:96–107

Liu X, Liang Z, Zhang Y et al (2018) Experimental study on the monitoring of rockburst in tunnels under dry and saturated conditions using AE and infrared monitoring. Tunn Undergr Sp Technol 82:517–528

Lockner D (1993) The role of acoustic emission in the study of rock fracture. Int J Rock Mech Min Sci Geomech Abstr 30:883–899

Ma L, Liu X, Wang M et al (2013) Experimental investigation of the mechanical properties of rock salt under triaxial cyclic loading. Int J Rock Mech Min Sci 62:34–41

Martin CD (1997) Seventeenth Canadian Geotechnical Colloquium: the effect of cohesion loss and stress path on brittle rock strength. Can Geotech J 34(5):698–725

Martin CD, Chandler N (1994) The progressive fracture of Lac du bonnet granite. Int J Rock Mech Min Sci Geomech Abstr 31(6):643–659

Momeni A, Karakus M, Khanlari G, Heidari M (2015) Effects of cyclic loading on the mechanical properties of a granite. Int J Rock Mech Min Sci 100(77):89–96

Munoz H, Taheri A (2019) Postpeak deformability parameters of localized and nonlocalized damage zones of rocks under cyclic loading. Geotech Test J 42(6):1663–1684

Munoz H, Taheri A, Chanda EK (2016a) Fracture energy-based brittleness index development and brittleness quantification by pre-peak strength parameters in rock uniaxial compression. Rock Mech Rock Eng 49(12):4587–4606

Munoz H, Taheri A, Chanda EK (2016b) Pre-peak and post-peak rock strain characteristics during uniaxial compression by 3D digital image correlation. Rock Mech Rock Eng 49(7):2541–2554

Royer-Carfagni G, Salvatore W (2000) The characterization of marble by cyclic compression loading: experimental results. Mech Cohes Frict Mater 5(7):535–563

Shirani Faradonbeh R, Taheri A (2019) Long-term prediction of rockburst hazard in deep underground openings using three robust data mining techniques. Eng Comput 35(2):659–675

Shirani Faradonbeh R, Taheri A, Karakus M (2020) Post-peak behaviour of rocks under cyclic loading using a double-criteria damage-controlled test method. Bull Eng Geol Environ 80(2):1713–1727

Singh SK (1989) Fatigue and strain hardening behaviour of graywacke from the flagstaff formation. New South Wales Eng Geol 26(2):171–179

Sufian A, Russell AR (2013) Microstructural pore changes and energy dissipation in Gosford sandstone during pre-failure loading using X-ray CT. Int J Rock Mech Min Sci 57:119–131

Taheri A, Tani K (2008) Use of down-hole triaxial apparatus to estimate the mechanical properties of heterogeneous mudstone. Int J Rock Mech Min Sci 45(8):1390–1402

Taheri A, Tatsuoka F (2015) Small- and large-strain behaviour of a cement-treated soil during various loading histories and testing conditions. Acta Geotech 10(1):131–155

Taheri A, Royle A, Yang Z, Zhao Y (2016a) Study on variations of peak strength of a sandstone during cyclic loading. Geomech Geophys Geo-Energy Geo Resour 2(1):1–10

Taheri A, Yfantidis N, Olivares LC et al (2016b) Experimental study on degradation of mechanical properties of sandstone under different cyclic loadings. Geotech Test J 39(4):673–687

Taheri A, Hamzah N, Dai Q (2017) Degradation and improvement of mechanical properties of rock under triaxial compressive cyclic loading. Jpn Geotech Soc Spec Publ 5:71–78

Taheri A, Zhang Y, Munoz H (2020) Performance of rock crack stress thresholds determination criteria and investigating strength and confining pressure effects. Constr Build Mater 243:118263

Tarasov B, Potvin Y (2013) Universal criteria for rock brittleness estimation under triaxial compression. Int J Rock Mech Min Sci 59:57–69

Trippetta F, Collettini C, Meredith PG, Vinciguerra S (2013) Evolution of the elastic moduli of seismogenic triassic evaporites subjected to cyclic stressing. Tectonophysics 592:67–79

Vasconcelos G, Lourenço P, Alves C, Pamplona J (2009) Compressive behavior of granite: Experimental approach. J Mater Civ Eng 21(9):502–511

Wang W, Wang M, Liu X (2016) Study on mechanical features of brazilian splitting fatigue tests of salt rock. Adv Civ Eng 2016:5436240

Wang S, Xu W, Sun M, Wang W (2019) Experimental investigation of the mechanical properties of fine-grained sandstone in the triaxial cyclic loading test. Environ Earth Sci 78(14):416

Wawersik WR, Fairhurst CH (1970) A study of brittle rock fracture in laboratory compression experiments. Int J Rock Mech Min Sci Geomech Abstr 7(5):561–575

Xiao JQ, Ding DX, Xu G, Jiang FL (2009) Inverted S-shaped model for nonlinear fatigue damage of rock. Int J Rock Mech Min Sci 3(46):643–648

Zhang D, Ranjith PG, Perera MSA (2016) The brittleness indices used in rock mechanics and their application in shale hydraulic fracturing: a review. J Pet Sci Eng 143:158–170

Zhang J, Deng H, Taheri A et al (2019) Deterioration and strain energy development of sandstones under quasi-static and dynamic loading after freeze-thaw cycles. Cold Reg Sci Technol 160:252–264

Zoback MD, Byerlee JD (1975) The effect of cyclic differential stress on dilatancy in westerly granite under uniaxial and triaxial conditions. J Geophys Res 80(11):1526–1530